Mon. Not. R. Astron. Soc. **000**, 1–?? (2011) Printed 9 November 2011 (MN LATEX style file v2.2)

Galaxy Zoo: Building the low-mass end of the red sequence with local post-starburst galaxies⋆

O.I. Wong,[1,2] K. Schawinski,[3,4,15] S. Kaviraj,[5,6] K.L. Masters,[7,8] R.C. Nichol,[7] C. Lintott,[9,6] W.C. Keel,[10] D. Darg,[6] S.P. Bamford,[11] D. Andreescu,[12] P. Murray,[13] M.J. Raddick,[14] A. Szalay,[14] D. Thomas,[7] J. VandenBerg[14]

[1]*CSIRO Astronomy & Space Science, P.O. Box 76 Epping, NSW 1710, Australia*
[2]*Astronomy Department, Yale University, P.O. Box 208101 New Haven, CT 06520-8101, U.S.A.*
[3]*Department of Physics, Yale University, New Haven, CT 06511, U.S.A.*
[4]*Yale Center for Astronomy and Astrophysics, Yale University, P.O. Box 208121, New Haven, CT 06520, U.S.A.*
[5]*Blackett Laboratory, Imperial College London, South Kensington Campus, London SW7 2AZ, U.K.*
[6]*Oxford Astrophysics, Department of Physics, University of Oxford, Denys Wilkinson Building, Keble Road, Oxford, OX1 3RH, U.K.*
[7]*Institute for Cosmology and Gravitation, Dennis Sciama Building, University of Portsmouth, Burnaby Road, Portsmouth, PO1 3FX, U.K.*
[8]*South East Physics Network, SEPnet, (www.sepnet.ac.uk)*
[9]*Adler Planetarium, 1300 S. Lakeshore Drive, Chicago, IL 60605, U.S.A.*
[10]*Department of Physics & Astronomy, 206 Gallalee Hall, 514 University Blvd., University of Alabama, Tuscaloosa, AL35487-0234, U.S.A.*
[11]*Centre for Astronomy & Particle Theory, University of Nottingham, University Park, Nottingham, NG7 2RD, U.K.*
[12]*LinkLab, 4506 Graystone Ave., Bronx, NY 10471, U.S.A.*
[13]*Fingerprint Digital Media, 9 Victoria Close, Newtownards, Co. Down, Northern Ireland, BT23 7GY, U.K.*
[14]*Department of Physics and Astronomy, The Johns Hopkins University, Homewood Campus, Baltimore, MD 21218, U.S.A.*
[15]*Einstein Fellow*

Released 2011 Xxxxx XX

ABSTRACT

We present a study of local post-starburst galaxies (PSGs) using the photometric and spectroscopic observations from the Sloan Digital Sky Survey (SDSS) and the results from the Galaxy Zoo project. We find that the majority of our local PSG population have neither early- nor late-type morphologies but occupy a well-defined space within the colour–stellar mass diagram, most notably, the low-mass end of the "green valley" below the transition mass thought to be the mass division between low-mass star-forming galaxies and high-mass passively-evolving bulge-dominated galaxies. Our analysis suggests that it is likely that a local PSG will quickly transform into "red", low-mass early-type galaxies as the stellar morphologies of the "green" PSGs largely resemble that of the early-type galaxies within the same mass range. We propose that the current population of PSGs represents a population of galaxies which is rapidly transitioning between the star-forming and the passively-evolving phases. Subsequently, these PSGs will contribute towards the build-up of the low-mass end of the "red sequence" once the current population of young stars fade and stars are no longer being formed. These results are consistent with the idea of "downsizing" where the build-up of smaller galaxies occurs at later epochs.

Key words: galaxies: evolution

1 INTRODUCTION

Current research in galaxy evolution is still largely driven by our lack of understanding of the link between the two main types of galaxies observed in the sky. Many theories exist to explain the evolution between star-forming, gas-rich spiral galaxies ("late"-type) and non-star-forming, passively-evolving spheroid galaxies ("early"-type). Since this bimodal nature is highly correlated to the stellar age and star formation history of the individual galaxies, it is likely that we are observing two main stages of galaxy evolution (Strateva et al. 2001; Baldry et al. 2004, 2006; Kauffmann et al. 2004; Drory et al. 2009); and that the transition between these two types occurs relatively quickly (Martin et al. 2007). The colours and brightnesses (as defined by their observed magnitudes) of all galaxies appear to be concentrated within two well-defined colour–

⋆ This publication has been made possible by the participation of more than 250,000 volunteers in the Galaxy Zoo project. Their contributions are individually acknowledged at `http://www.galaxyzoo.org/Volunteers.aspx`.

magnitude regions. The star-forming galaxies appear to populate a space dubbed the "blue cloud" and the passively-evolving, non star-forming galaxies lie in a region called the "red sequence". Recent studies argue that local galaxies must migrate rapidly (within a Gyr) from the "blue cloud" to the "red sequence"[1] due to the scarcity of galaxies within the intervening parameter space (occasionally dubbed the "green valley"; e.g. Schawinski et al. 2007). Therefore, valuable insights into galaxy evolution can be obtained by studying galaxies that appear to have intermediate properties and may be in the act of transitioning between the two main galaxy populations.

Post-starburst galaxies (hereafter PSGs) or post-quenching galaxies (Yan et al. 2009) such as "E+A" or "K+A" galaxies, are galaxies which appear to have ceased current star formation, but still exhibit the spectral signature of recently-formed stars. In E+A galaxies, strong Balmer absorption lines are observed together with α-element signatures such as Mg_{5175}, Fe_{5270} and $Ca_{3934,3468}$ (Dressler & Gunn 1983, 1992; Dressler et al. 1999, 2004; Couch & Sharples 1987; MacLaren et al. 1988; Newberry et al. 1990; Fabricant et al. 1991; Abraham et al. 1996; Poggianti et al. 1999; Goto et al. 2003; Goto 2004, 2005, 2007). Similar to E+A galaxies, K+A galaxies are PSGs which have a disk-like morphology (Couch et al. 1994; Dressler et al. 1994; Caldwell & Rose 1997; Dressler et al. 1999). Although PSGs such as E+A galaxies are more common at higher redshifts (Wild et al. 2009; Tran et al. 2004), detailed high-resolution studies are only possible with a local population of PSGs since low redshift observations extend to lower surface brightness limits than that at earlier epochs.

Current studies favor the idea that PSGs are formed via interactions or major mergers (Yamauchi et al. 2008; Blake et al. 2004; Bekki et al. 2001) which trigger bursts of star formation. However, due to the effects of the merger interaction, the gas reservoir (from which stars are formed) is depleted and these PSGs eventually turn into bulge-dominated early-type galaxies once their star formation fades completely (e.g. Yang et al. 2008). Kaviraj et al. (2007) found that the quenching efficiency of star formation in less massive ($< 10^{10}$ $M_{\odot}$) and more massive E+A galaxies ($> 10^{10} M_{\odot}$) is consistent with supernovae (SNe) and AGN being the main sources of negative feedback, respectively.

Using the Sloan Digital Sky Survey (SDSS), we assemble and analyze one of the largest, and most complete samples, of local PSGs to date. This paper investigates the properties of the local PSGs derived from the visual classifications of the Galaxy Zoo citizen science project (Lintott et al. 2010, 2008).

Section 2 describes our sample selection and the sample properties are examined in Section 3. A discussion of our results and conclusions can be found in Section 4. The AB magnitude system is used throughout this work.

[1] There are a few cases where the evolution of individual galaxies moves from the "red sequence" to the "blue cloud" (e.g. Kannappan et al. 2009; Wei et al. 2010). In these cases, passively-evolving galaxies have accreted more gas recently and are in the process of regrowing their stellar disk. However, this "red-to-blue" mode of evolution is very unlikely to apply to our particular study because our PSGs are defined to have no current on-going star formation.

2 OUR GALAXY SAMPLE

In this paper, we obtain the photometric and spectroscopic data from the Sloan Digital Sky Survey (SDSS) DR7 (York et al. 2000; Abazajian et al. 2009) for all objects classified as 'galaxy' (Strauss et al. 2002). The main galaxy emission line measurements are determined from the SDSS spectra using the `Gandalf` IDL tool by Sarzi et al. (2006). To minimise the Malmquist bias, and create a volume and magnitude-limited (proxy for stellar-mass limited) sample of galaxies, we select all the galaxies within $0.02 < z < 0.05$ with $M_{z,Petro} < -19.5$ magnitudes. We use the z-band since the reddest waveband provides the closest proxy to stellar mass. It should be noted that the results of this paper remain unchanged if the i-band is used instead. As we aim to study the properties of all galaxies which have ceased star formation recently, we define a PSG to be a galaxy with a recently-truncated star formation history (i.e. where the observed Hα emission line is weaker than four times the RMS level), while still exhibiting strong balmer absorption lines from recently-formed young stars (where the Hδ equivalent width is wider than three Angstroms). Our strict Hα criterion may result in the omission of a few PSG known to emit weak Hα emission but the effects from the inclusion of a few Hα-emitting galaxies do not change any of the results that we present in Section 3.

Studies such as Balogh et al. (1999); Blake et al. (2004); Goto (2007) select for PSGs at higher redshifts ($0.5 < z < 1.0$) which exhibit very strong A-type stellar populations (where the observed Hδ equivalent width is wider than five Angstroms). To include as many PSGs as possible into our sample, we imposed a more relaxed Hδ equivalent width so we do not bias against galaxies with a low star formation rate (which results in weaker Balmer equivalent widths) prior to the cessation of star formation.

The [OII] forbidden lines were not used in the selection criteria because the Hα emission line is a more accurate tracer of current star formation in the Local Universe. The luminosity of the [OII] emission lines is not directly linked to the ionizing luminosity and the [OII] excitation is sensitive to the abundance and the ionisation state of the gas (Kennicutt 1998). Moreover, the [OII]-derived star formation rates (SFRs) is sensitive to systematic errors from extinction and variations in the diffused gas fraction (Kennicutt 1998). In starburst galaxies, the excitation of [OII] is much higher in the diffused ionised gas (Hunter & Gallagher 1990; Hunter 1994; Martin 1998), and is able to double the L[OII]/SFR ratio in the integrated spectrum (Kennicutt 1992).

Of 47,573 galaxies within our selected volume, we find a total of 80 PSGs. The general properties of our PSGs are listed in Table 1. Figure 1 shows the SDSS multicolour composite images for 12 random PSGs within our sample. This figure exhibits the variety of morphologies and sizes within our PSG sample.

Using the bootstrap resampling method to approximate the uncertainty, we find that our percentage of PSGs to the total number of galaxies (within our specified volume out to $z \sim 0.05$) is $0.17^{+0.07}_{-0.05}$ %. This assumes that the uncertainty in our spectral line measurements is given by the signal-to-noise ratio (SNR). This PSG fraction is comparable to that of previous local PSG studies by Goto (2005, 2007) and Kaviraj et al. (2007). It should be noted that we do not find many of the E+A galaxies found by Goto (2005, 2007) (hereafter known as the "G05" sample) from the SDSS DR5 catalogue because we detect strong Hα emission in these G05 objects using the SDSS DR7 catalogue. Hence, these E+A galaxies appear to have current, on-going star formation and is inconsistent with our definition of a PSG. Of the overlap galaxies between our full galaxy

Table 2. Distributions of galaxy morphologies and star formation properties of our entire local volume sample and that of the PSG sample. The distributions are listed as percentages and the number of galaxies are given in parentheses.

	Entire Galaxy Sample			PSG sample
	Non-SF	SF	Total	
Early-type	50% (5148)	10% (3770)	19% (8918)	16% (13)
Intermediate	46% (4841)	47% (17589)	47% (22430)	74% (59)
Late-type	4% (388)	43% (15837)	34% (16225)	10% (8)
Total	100% (10377)	100% (37196)	100% (47573)	100% (80)

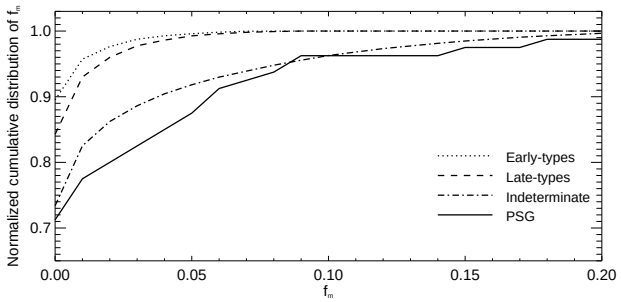

Figure 2. Peak-normalized cumulative distributions of $f_{\rm m}$ for our PSG sample (black solid line) and the different types of galaxies within the control sample.

sample and that of the G05 sample, we find that our method of using the Balmer absorption line strength finds every galaxy found via its absorption line equivalent width. This is consistent with the fact that there is a good correlation between the line strengths and the equivalent widths for galaxies of similar sizes.

3 RESULTS

3.1 Morphological properties

3.1.1 Morphological classification using Galaxy Zoo

Galaxy morphologies are derived from the Galaxy Zoo 1 project (Lintott et al. 2010). From the multiple independent inspections (and classifications) made for each galaxy, the accuracy of the classifications for individual galaxies can be determined by imposing a required level of agreement among the classifiers. Following the definition of the `clean` sample from Land et al. (2008), we require a minimum of an 80% majority agreement on the morphology for each object. Spiral galaxies (from an Sa to an Sd morphology) are classified as *late-type* objects, while all spheroids (including lenticular galaxies) are classed as *early-type*. Galaxy morphologies which are neither "early"- nor "late" are classed as *intermediate-type* which include galaxies with irregular/disturbed and merging morphologies.

Relative to the entire local volume sample, there is a smaller fraction of PSGs with spiral or late-type morphologies. We find that 74 ($\pm$10)% of our PSG sample appear to have intermediate morphologies, while 16 ($\pm$5)% and 10 ($\pm$4)% of our PSGs are classed as early- and late-types, respectively. It should be noted that a colour bias in morphology votes (by the Galaxy Zoo citizen scientists) is unlikely to occur since our PSG sample is dominated by intermediate-type morphologies. In addition, investigations by Lintott et al. (2008) found colour bias to not be a significant effect on the final morphological classifications.

Similar to the results of Baldry et al. (2004); Driver et al. (2006); Bamford et al. (2009), we find that the majority of the spheroidal/elliptical galaxies within our local volume sample exhibit non-star-forming (non-SF) properties, while, the star-forming (SF) galaxies tended to have spiral morphologies. In this paper, we classify a galaxy as star-forming if its Hα emission line is stronger than four times the RMS level. As expected from our PSG selection criteria of galaxies with recently-truncated star formation, we find that the PSGs appear to have a morphology distribution which appears intermediate to that of SF and non-SF galaxies within the control sample. Table 2 lists the distribution of morphologies and star-forming properties of both the local volume control sample and the PSG sample.

In addition to the Galaxy Zoo classifications, we visually inspected each PSG to confirm the morphologies. Consistent with the fact that a majority of the PSGs have intermediate-type morphologies, we find disturbed galaxy morphologies which resemble neither early- nor late-type galaxies. Depending on the size of the galaxy, the 3″ fibers (from which the SDSS spectra are obtained) may only correspond to the central 1.2–2.9 kpc of galaxies within our redshift range. In our sample, the observed spectral properties may not be representative for approximately 5% of our sample where the outer galaxy regions are much greater than 3″ and appear to be bluer than the central region.

The $f_{\rm m}$ parameter is a quantification of the merger properties of Galaxy Zoo 1 and is defined to be the weighted-merger-vote fraction where the fraction of merger votes is multiplied by a weighting factor (W; Lintott et al. 2008) to account for the quality of the particular voters who have assessed each galaxy (Darg et al. 2010). Assuming that $f_{\rm m} > 0.4$ describes a merger (Darg et al. 2010), we do not find many mergers within our PSG sample even though a large number of the PSGs appear asymmetrical or disturbed. A comparison of the distribution of $f_{\rm m}$ parameters of our PSG sample to those of the early- and late-types of the entire galaxy sample yields Kolmogorov-Smirnov (KS) probabilities which indicate that there are no significant differences between any of the $f_{\rm m}$ distributions. Figure 2 shows the normalized cumulative distributions of $f_{\rm m}$ for the different galaxy types.

3.1.2 Concentration

As the majority of our PSG sample consists of intermediate-type morphologies, further investigation of the stellar structure will reveal quantitatively whether these PSGs truly have intermediate-type morphologies (possibly due to past interactions) or are similar in structure to the early- or late-type galaxies within the same volume. We measure the concentration index using the ratio between the $R90$ and $R50$ parameters which are the radii where 90% and 50% of the total Petrosian[2] flux have been measured in the i-band. Therefore bulge-dominated galaxies will have greater $R90/R50$ ratios, while disk-dominated galaxies will have smaller values.

To determine the end-products of our PSG sample, we compare the peak-normalised distributions of concentration indices

[2] A Petrosian radius is where the mean local surface brightness (within the local annulus) is equal to a constant fraction of the mean surface brightness within that radius (Strauss et al. 2002).

Table 1. General properties of our PSG sample.

SDSS object ID (1)	RA (2)	Declination (3)	m_r (4)	$u-r$ (5)	$EW(\mathrm{H}\delta)$ (6)	$S_{[\mathrm{OII}]}$ (7)	$S_{\mathrm{H}\alpha}$ (8)	log (M$_\star$) (9)	f_m (10)	$frac_{\mathrm{dev}}$ (11)	Type (12)	Comments
587731513679478898	01:14:47.2	+00:37:55.7	16.75	2.00	3.4	$< 7.9 \times 10^{-15}$	—	9.95	0.000	0.595	I	—
587731513681313986	01:31:37.9	+00:48:51.7	16.52	1.37	5.0	$< 2.4 \times 10^{-16}$	$< 1.3 \times 10^{-17}$	9.69	0.000	0.000	I	—
587731511533961332	01:32:50.2	−00:56:17.6	16.86	2.11	4.7	$< 6.4 \times 10^{-15}$	$< 1.5 \times 10^{-15}$	10.03	0.000	1.000	I	blob
587727230522032233	01:37:16.4	−09:29:06.5	16.63	2.25	3.7	$< 1.2 \times 10^{-16}$	—	9.96	0.000	0.546	I	blob
588015510358524013	02:20:38.7	+00:54:09.1	15.15	0.97	4.1	1.5×10^{-13}	$< 6.3 \times 10^{-15}$	9.66	0.000	0.240	S	—
587731512082956346	03:23:33.3	−00:26:18.8	14.92	2.04	4.2	—	$< 7.3 \times 10^{-14}$	9.99	0.000	0.770	E	—
587731514232996008	03:47:10.2	+01:04:39.9	15.78	1.77	3.9	$< 4.8 \times 10^{-16}$	$< 4.7 \times 10^{-17}$	9.97	0.000	0.007	I	—
587732053779283987	08:43:20.7	+37:13:27.6	16.24	2.26	3.7	$< 5.5 \times 10^{-16}$	$< 3.1 \times 10^{-16}$	10.23	0.000	0.926	I	blob
587744874791370929	09:01:03.8	+13:36:33.3	14.91	0.85	4.0	1.7×10^{-13}	$< 1.2 \times 10^{-14}$	9.82	0.188	0.505	I	disturbed
587745403073855572	09:11:31.1	+12:08:52.1	14.96	2.22	3.3	$< 1.0 \times 10^{-14}$	$< 2.4 \times 10^{-15}$	10.43	0.047	1.000	I	disturbed
587745540514119842	09:25:03.2	+13:03:58.0	16.56	2.06	3.0	$< 3.5 \times 10^{-14}$	$< 2.2 \times 10^{-15}$	9.81	0.000	1.000	I	blob
588016891707392070	09:29:34.6	+33:47:51.1	15.28	1.22	4.3	1.1×10^{-13}	$< 1.6 \times 10^{-14}$	9.70	0.115	0.000	I	disturbed
587745243626405989	09:45:00.0	+15:27:40.0	15.79	2.10	4.0	$< 1.2 \times 10^{-14}$	$< 4.2 \times 10^{-15}$	10.25	0.000	0.609	I	blob
587735044693753946	09:46:29.9	+39:02:19.7	16.72	1.34	3.9	1.9×10^{-13}	$< 1.2 \times 10^{-14}$	9.61	0.000	0.620	I	—
587725074458804315	09:49:56.4	−00:13:52.9	13.89	2.36	3.4	$< 6.5 \times 10^{-16}$	$< 2.7 \times 10^{-16}$	11.35	0.095	1.000	I	disturbed
588848909073789221	10:04:29.8	+00:41:20.2	16.49	2.06	3.2	$< 1.8 \times 10^{-16}$	$< 2.1 \times 10^{-16}$	9.93	0.000	0.870	I	blob
587726032236183669	10:06:50.9	+01:41:34.0	16.94	2.08	5.7	$< 2.0 \times 10^{-16}$	—	9.84	0.074	0.613	I	blob
587738948283334792	10:12:18.9	+36:07:50.0	15.62	1.59	3.3	1.1×10^{-13}	$< 1.9 \times 10^{-14}$	9.96	0.000	0.964	I	blob
587741828579393617	10:21:25.9	+21:32:45.8	16.00	1.90	4.1	—	$< 6.2 \times 10^{-16}$	9.91	0.000	0.002	S	—
587733080268931236	10:30:53.7	+51:19:59.6	15.05	1.18	4.2	4.9×10^{-15}	$< 8.3 \times 10^{-16}$	10.35	0.031	0.194	S	asymmetric
587728947978436717	10:42:32.3	−00:41:58.3	15.83	2.07	4.3	$< 2.9 \times 10^{-16}$	$< 7.5 \times 10^{-16}$	10.10	0.000	0.994	I	blob
587729386611212446	10:53:05.4	+57:51:54.2	15.60	1.10	3.8	3.7×10^{-16}	$< 1.5 \times 10^{-16}$	10.05	0.000	0.054	I	—
587734894357381314	11:00:48.5	+10:31:19.0	16.44	2.23	4.2	$< 6.1 \times 10^{-15}$	$< 1.6 \times 10^{-15}$	10.12	0.000	0.864	I	asymmetric
587741489834754106	11:10:33.9	+28:29:33.3	15.73	2.07	4.1	—	$< 1.4 \times 10^{-14}$	10.00	0.000	0.985	I	blob
588848898833842380	11:13:28.0	−00:54:09.5	16.62	2.03	4.9	$< 2.5 \times 10^{-14}$	$< 3.7 \times 10^{-15}$	9.57	0.000	0.771	I	blob
587732580982521898	11:19:07.6	+58:03:14.3	14.17	2.16	4.7	1.6×10^{-13}	$< 2.9 \times 10^{-14}$	10.74	0.000	1.000	I	asymmetric
587739405703577638	11:26:53.7	+33:07:09.5	14.86	1.21	4.5	1.3×10^{-13}	$< 7.3 \times 10^{-15}$	9.92	0.108	0.190	S	—
587732482746548338	11:35:32.0	+48:56:38.5	15.99	2.19	4.0	$< 6.5 \times 10^{-15}$	$< 1.3 \times 10^{-15}$	9.76	0.017	0.866	I	disturbed
587741726574444657	11:36:55.2	+24:53:25.5	14.92	1.73	5.5	1.4×10^{-13}	$< 5.0 \times 10^{-11}$	9.98	0.027	0.200	I	disturbed
587742573224657026	11:43:47.8	+20:21:48.0	15.61	1.83	6.7	$< 8.2 \times 10^{-15}$	—	9.56	0.000	0.305	S	disturbed
588017111833182222	12:21:05.7	+47:58:51.9	16.54	2.18	3.6	$< 7.2 \times 10^{-14}$	$< 2.2 \times 10^{-15}$	10.02	0.000	0.978	I	—
588017730836561977	12:26:41.6	+08:44:32.2	15.42	2.45	6.5	$< 8.9 \times 10^{-13}$	$< 4.9 \times 10^{-14}$	10.38	0.000	0.906	I	—
587726033325850747	12:32:18.9	+03:00:09.8	16.82	2.00	3.3	$< 6.2 \times 10^{-14}$	—	10.10	0.000	1.000	I	blob
587725816414142618	12:32:23.3	+66:25:36.6	16.90	2.26	3.1	$< 1.0 \times 10^{-16}$	—	9.82	0.032	0.528	I	blob
587734892220252284	12:37:18.0	+09:32:09.0	14.55	1.89	3.0	$< 3.4 \times 10^{-16}$	—	9.84	0.000	0.979	E	—
587739096454332452	12:38:52.8	+36:32:05.7	15.74	2.15	3.7	$< 1.2 \times 10^{-16}$	$< 1.3 \times 10^{-17}$	10.19	0.000	1.000	E	—
587741602572599308	12:57:17.8	+27:48:39.3	15.40	1.97	3.9	$< 1.7 \times 10^{-15}$	$< 4.4 \times 10^{-18}$	9.74	0.000	0.211	I	disturbed
587741722823557134	12:57:21.7	+27:52:49.5	15.23	2.10	3.6	$< 5.1 \times 10^{-15}$	$< 1.9 \times 10^{-17}$	9.94	0.000	0.873	E	—
587741722286686489	12:57:45.7	+27:25:45.6	15.92	1.94	3.9	$< 1.3 \times 10^{-13}$	$< 1.1 \times 10^{-14}$	9.56	0.000	0.254	S	—
587741721749881039	12:58:12.0	+27:07:39.5	16.60	2.31	3.5	$< 3.0 \times 10^{-14}$	—	10.06	0.000	0.806	S	—
587741722823754043	12:59:39.5	+27:51:16.6	16.57	2.20	4.2	$< 3.7 \times 10^{-17}$	$< 1.1 \times 10^{-17}$	9.95	0.454	0.343	I	disturbed
587741722823819345	13:00:10.2	+27:51:50.2	15.85	2.22	3.4	$< 2.8 \times 10^{-15}$	—	10.00	0.097	0.357	I	disturbed
587741722286948519	13:00:29.2	+27:30:53.4	15.53	1.63	8.5	$< 1.1 \times 10^{-15}$	$< 9.6 \times 10^{-17}$	9.55	0.125	0.224	I	disturbed
587739719754514434	13:04:22.7	+28:48:38.8	14.33	0.86	4.4	$< 2.9 \times 10^{-12}$	$< 4.2 \times 10^{-14}$	10.15	0.365	0.643	S	disturbed
587733195160485975	13:05:25.8	+53:35:30.3	14.29	2.15	4.6	$< 4.8 \times 10^{-16}$	$< 1.4 \times 10^{-16}$	10.75	0.000	1.000	E	—
587722982822379684	13:17:59.6	−00:17:43.2	13.29	1.22	5.2	$< 2.1 \times 10^{-14}$	$< 5.1 \times 10^{-14}$	10.44	0.139	0.477	S	asymmetric
587729773681377291	13:37:44.1	−02:10:27.9	14.61	0.72	3.5	—	$< 2.5 \times 10^{-14}$	10.41	0.000	0.338	S	—
587726032797565040	13:50:51.0	+02:19:38.5	15.62	2.11	4.7	$< 3.2 \times 10^{-16}$	$< 8.7 \times 10^{-17}$	9.97	0.167	1.000	I	disturbed
587730021178867826	14:18:51.0	+05:28:14.2	15.92	2.09	3.0	$< 7.3 \times 10^{-15}$	$< 2.6 \times 10^{-15}$	9.90	0.000	0.961	I	blob
587739827130007710	14:39:08.5	+22:17:42.4	15.42	0.84	4.5	2.0×10^{-14}	$< 1.1 \times 10^{-15}$	9.75	0.136	0.000	I	asymmetric
587739408405626997	14:39:30.4	+30:52:49.1	16.14	1.97	4.2	$< 5.0 \times 10^{-14}$	$< 1.3 \times 10^{-15}$	9.97	0.153	1.000	I	disturbed
587739379916210254	14:54:24.7	+27:39:38.7	16.23	2.04	3.9	$< 1.8 \times 10^{-16}$	$< 4.2 \times 10^{-17}$	9.98	0.000	1.000	I	blob
587726032268362094	15:01:24.0	+01:39:25.0	15.90	1.92	3.9	—	$< 4.5 \times 10^{-15}$	9.95	0.000	0.682	I	blob
588017949366157511	15:03:39.4	+35:27:30.5	16.14	0.94	3.9	1.8×10^{-13}	$< 6.4 \times 10^{-15}$	9.60	0.000	0.000	I	—
587736975271067720	15:12:04.1	+28:25:14.1	14.26	1.20	4.2	1.3×10^{-15}	$< 4.7 \times 10^{-15}$	10.43	0.015	0.772	I	asymmetric
588017991773978739	15:14:29.9	+07:35:46.8	15.45	1.97	4.4	$< 4.7 \times 10^{-14}$	$< 5.5 \times 10^{-15}$	10.27	0.000	0.918	I	blob
587736543098568963	15:21:08.6	+07:37:53.9	16.40	2.05	4.9	$< 1.7 \times 10^{-14}$	$< 2.5 \times 10^{-15}$	10.12	0.000	0.920	I	blob
587742575924805956	15:23:22.8	+13:26:19.2	15.91	1.38	3.4	2.8×10^{-14}	$< 7.7 \times 10^{-15}$	9.99	0.000	0.038	I	disturbed
587736477596975155	15:23:43.0	+08:27:29.0	15.86	2.06	3.0	$< 5.2 \times 10^{-16}$	—	9.81	0.000	1.000	I	—
587739810494218509	15:24:25.6	+19:42:59.5	14.96	1.13	5.4	1.2×10^{-14}	$< 1.4 \times 10^{-15}$	9.73	0.027	0.031	S	L; disturbed
587733603187556413	15:26:21.9	+48:42:14.4	15.88	1.58	3.9	1.4×10^{-13}	$< 5.7 \times 10^{-14}$	10.07	0.310	1.000	I	—
588017703489634681	15:26:53.3	+08:32:07.7	16.64	2.21	4.7	$< 1.3 \times 10^{-13}$	$< 5.7 \times 10^{-15}$	10.00	0.000	0.359	I	blob
587730021724062009	15:34:53.4	+04:16:60.0	15.66	1.43	3.5	1.9×10^{-15}	$< 7.4 \times 10^{-16}$	10.00	0.000	0.181	I	disturbed
587739721917595889	15:39:19.9	+21:21:30.0	16.76	2.05	3.1	$< 3.9 \times 10^{-15}$	$< 8.8 \times 10^{-16}$	9.86	0.000	1.000	I	blob
588017704565276972	15:44:31.7	+08:35:07.4	16.52	1.93	3.6	$< 6.4 \times 10^{-14}$	$< 3.3 \times 10^{-15}$	9.75	0.000	0.717	S	—
588011101570662666	16:00:17.3	+46:51:35.6	16.57	2.28	3.3	$< 9.8 \times 10^{-14}$	$< 8.1 \times 10^{-15}$	10.29	0.000	0.779	E	blob
587739828212793702	16:03:15.7	+16:19:07.9	15.86	2.09	3.6	3.1×10^{-14}	$< 4.5 \times 10^{-15}$	10.07	0.044	0.814	I	disturbed
587739809961804053	16:03:25.9	+15:38:48.2	15.43	0.84	4.0	5.7×10^{-14}	$< 4.2 \times 10^{-15}$	9.55	0.000	0.106	S	L
587729227152752660	16:03:44.5	+52:24:12.6	15.57	2.23	4.3	$< 5.8 \times 10^{-15}$	$< 1.2 \times 10^{-15}$	10.42	0.000	1.000	E	—
587739707420901722	16:04:38.6	+17:36:35.0	16.61	2.00	3.8	$< 3.3 \times 10^{-17}$	$< 1.5 \times 10^{-16}$	9.46	0.186	0.499	I	disturbed
587725817501712592	16:16:52.9	+50:57:04.6	14.69	2.73	4.0	—	$< 6.7 \times 10^{-15}$	11.47	0.000	0.734	E	—
587735666928844900	16:25:18.3	+37:56:40.6	15.03	2.12	3.2	$< 1.0 \times 10^{-15}$	$< 1.6 \times 10^{-16}$	10.15	0.000	1.000	I	—
588018090548920817	16:41:33.5	+24:42:14.2	16.01	2.02	4.1	$< 6.9 \times 10^{-15}$	$< 2.3 \times 10^{-15}$	10.04	0.000	0.849	I	blob
588018253228408956	16:53:14.4	+25:07:59.2	14.01	1.45	4.3	1.1×10^{-13}	$< 9.3 \times 10^{-14}$	10.44	0.000	0.692	S	disturbed
588018254302609790	16:59:33.1	+24:55:59.9	16.17	2.36	3.0	$< 7.3 \times 10^{-16}$	$< 2.2 \times 10^{-16}$	10.28	0.000	0.717	I	blob
587733432998559923	17:04:51.3	+25:03:18.4	16.51	2.51	8.3	$< 1.1 \times 10^{-14}$	$< 2.4 \times 10^{-15}$	10.45	0.068	1.000	I	blob
587725503947735340	17:14:07.2	+57:28:38.7	16.00	2.10	3.2	$< 1.4 \times 10^{-14}$	$< 8.2 \times 10^{-16}$	9.83	0.000	0.129	S	—
587731174382502294	21:19:48.2	+00:40:21.8	16.37	1.83	5.5	$< 3.7 \times 10^{-16}$	$< 5.5 \times 10^{-17}$	9.91	0.000	0.880	I	—
587727213347799419	21:33:56.5	−07:54:08.7	15.22	1.14	4.4	$< 2.7 \times 10^{-16}$	$< 5.5 \times 10^{-17}$	9.75	0.000	0.000	I	—
587731185117954089	22:08:06.1	−00:54:25.0	15.10	2.06	4.3	$< 4.9 \times 10^{-16}$	$< 3.3 \times 10^{-16}$	10.54	0.036	1.000	E	disturbed

Col. (1): SDSS object identification. Col. (2): Galaxy center's right ascension. Col. (3): Galaxy center's declination. Col. (4): r-band magnitude. Col. (5): $u-r$ colour. Col. (6): Hδ equivalent width (Angstroms). Col. (7): Measured [OII] flux densities in units of 10^{-17} ergs s^{-1} cm^{-2} Å^{-1}. The upper limits are defined to be four times the RMS noise. Col. (8): Estimated upper limits for the Hα flux densities in units of 10^{-17} ergs s^{-1} cm^{-2} Å^{-1} as defined to be four times the RMS noise. Col. (9): Log of the stellar mass obtained from Schawinski et al. (2007) which were determined by fitting the five SDSS photometric bands to model star formation histories from Maraston (1998, 2005) stellar models . Col. (10): Weighted merger parameter (Darg et al. 2010). Col. (11): The SDSS parameter which gives the fraction of light (in the r-band) fitted by a de Vaucouleurs profile. Col. (12): Description of galaxy type where 'S' represents late-type spiral galaxies, 'E' represents early-type galaxies and 'I' represent intermediate-type galaxies. Col. (10): Comments from visual inspection of each galaxy. A 'disturbed' comment indicates that the stellar morphology appears to have been disrupted by tidal interaction with features such as stellar tails/rings or with neighboring galaxies at close proximities. An 'asymmetric' defines an observed asymmetric stellar disk. A '—' comment represents galaxies whose morphologies appear fairly regular, while a 'blob' comment refers to galaxy morphologies which are small, compact and fairly spherical in appearance. An 'L' indicates that this galaxy exhibits spectral signatures of a LINER.

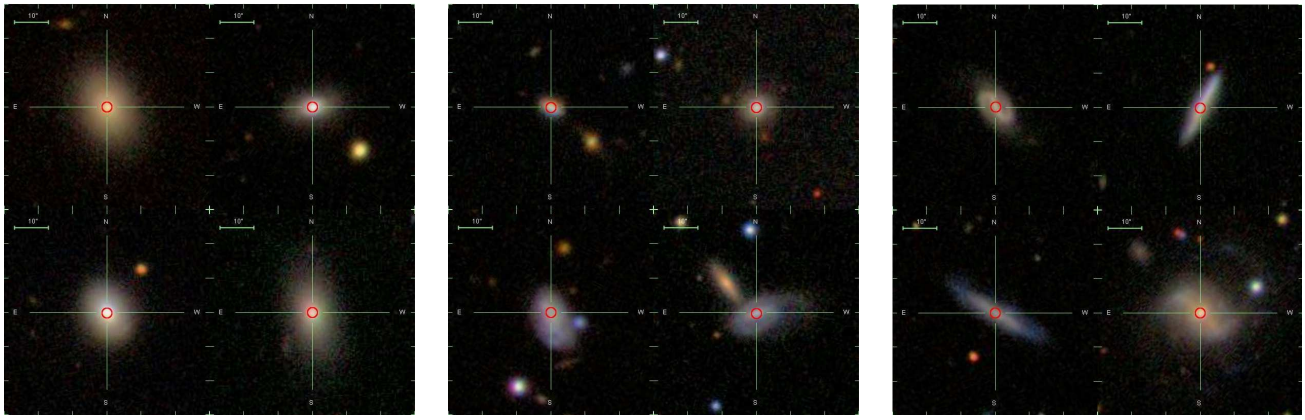

Figure 1. Example SDSS colour images of 12 PSGs within our sample. Each image frame provides a $48'' \times 48''$ field-of-view centered on the galaxy. The left panel shows four examples of early-type PSGs, the middle panel shows four examples of intermediate-type PSGs and the right panel shows four examples of late-type PSGs. The red circles show the SDSS fiber field-of-view where each spectrum was obtained.

for our population of PSGs to the early- and late-type population of galaxies with log ($M_\star$) < 10.5 $M_\odot$. In agreement with Strateva et al. (2001), we find that the division between early- and late-type galaxies is where the $R90$ is approximately 2.6 times greater than the $R50$. The distribution of concentration indices for our PSG sample is very similar to that of the early-type galaxies.

On the other hand, Masters et al. (2010) showed that early-type galaxies classified in such a manner may be contaminated by up to 50% by edge-on spirals and that the SDSS `fracDev` parameter (`fracDev`; which gives the fraction of light fitted by a de Vaucouleurs profile) provides a better differentiation between the early- and late-type galaxies as typical early-type elliptical galaxies are traditionally characterised by a de Vaucouleurs profile and as such have an `fracDev` > 0.5. As such, we show the distribution of `fracDev` for our "green" PSGs and low-mass early- and late-type sample in Figure 3. The PSG distribution is shown by the gray-shaded histogram, while the striped histogram in the left-panel represents the distribution for the early-types and the distribution for late-types are represented by the striped histogram in the right panel. A quantitative comparison using the KS test yields a KS probability of 0.68 that the `fracDev` distributions of PSGs and early-types are derived from the same parent sample, while the `fracDev` distributions of PSGs and late-types yield a KS probability of $<$0.001.

Therefore, we find that the structural stellar morphologies of the PSGs within the "green valley" appear to be more closely related to the morphologies of low-mass early-type galaxies even though star formation has only been truncated recently.

3.2 Colour and stellar mass

We derive the $u - r$ colours of our sample using the `modelMags` (from SDSS DR7; Abazajian et al. 2009) which are determined from the best fit of each galaxy profile to the linear combination of the exponential and the de Vaucouleurs profiles. In addition, these magnitude measurements are corrected for dust attenuation using the models of Calzetti et al. (2000). The "green valley" of our sample's colour distribution is defined to be within the nominal colour range of $1.8 < u - r < 2.3$. The stellar mass estimates for each galaxy are measured by fitting the five optical wavebands from SDSS to star formation history libraries generated from stellar models of Maraston (1998, 2005). The uncertainties in our derived

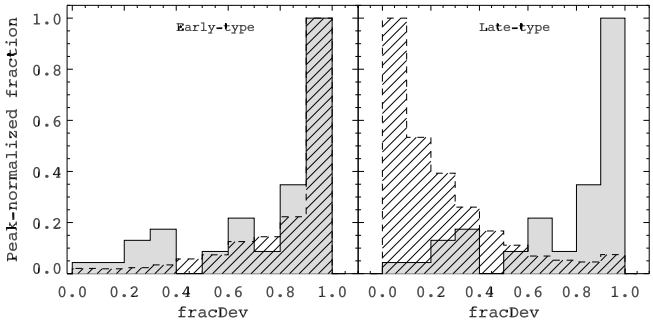

Figure 3. Peak-normalised distributions of `fracDev` (which describes the fraction of light from a fit to a de Vaucouleurs profile). The gray shaded histograms show the `fracDev` distribution for PSGs. The striped histogram show the `fracDev` distribution for the early-type galaxies (in the left panel) and the distribution for the late-type galaxies (in the right panel).

stellar masses are dominated by the inherent uncertainties within the stellar models used. More details on the parameterization of the star formation histories and the fitting process can be found in Schawinski et al. (2010) and references within.

The top row of panels in Figure 4 shows the colour–stellar mass distribution of our PSG sample as red solid circles and the SDSS galaxy sample of a particular type is represented by the black solid contours. Black dotted-lined contours represent the distribution of the entire sample regardless of galaxy-type and are shown for comparison purposes. The bottom row of panels in Figure 4 shows the distribution of the fraction of PSGs to the number of galaxies (of a particular type) in a given colour–stellar mass bin as a solid orange-shaded contour map overlaid on the solid contours showing the distribution of the SDSS galaxies of a particular type.

As can be seen from the top row panels of Figure 4, our PSG sample appears to be spread over a fairly large $u - r$ colour range even though a majority (94%) of the PSGs have stellar masses below the transition mass of log $M_\star < 10.5$ $M_\odot$ which separate the low-mass star-forming galaxies from the high-mass passively-evolving bulge-dominated galaxies (Kauffmann et al. 2003). In fact, we do not find any PSG with a log $M_\star > 11.5$ $M_\odot$. Such a stellar mass limit in our PSG sample is more clearly illustrated by the number fractions of PSGs to the number of galaxies within a

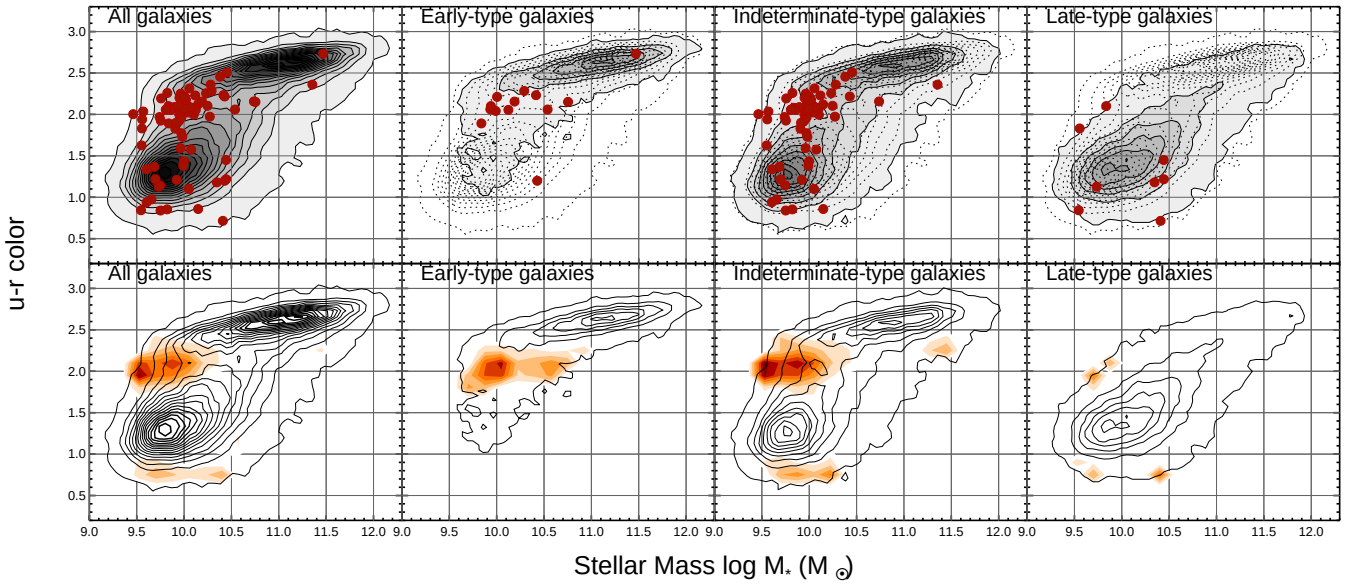

Figure 4. The $u-r$ colour versus stellar mass distribution of our the SDSS galaxy sample are shown by the contours. The top row shows PSG sample (solid red circles) overplotted onto the distribution of SDSS galaxies of a particular type (demarcated by the solid line contours). The panels from left to right show the distributions: for all galaxy types, for early-type galaxies, for intermediate-type galaxies and for late-type galaxies. Within the top row, the distribution of SDSS galaxies for all galaxy types are also shown as a comparison by dotted-lined contours within the early-, intermediate and late-type galaxy panels. The bottom row shows the number fraction of our PSG sample to the galaxy sample of a particular type in a given colour–mass bin as a solid orange contour map overlaid onto the contours marking the distribution of SDSS galaxies. The maximum number fractions for all galaxy types, early-types, intermediate-types, late-types are 3.0%, 2.6%, 3.0% and 1.9%; respectively.

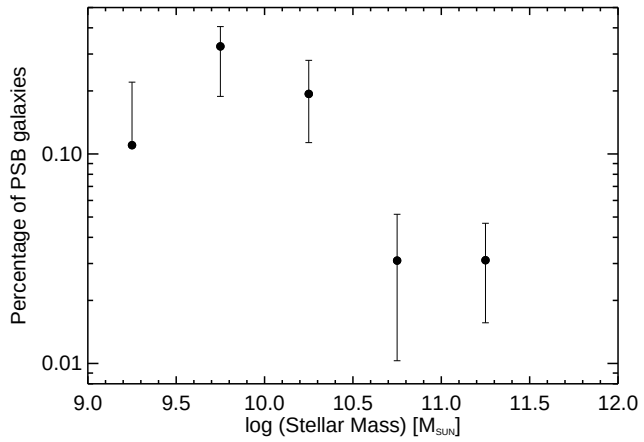

Figure 5. Percentage of PSGs as a function of stellar mass. The uncertainties are given by the $10^{\rm th}$ and $90^{\rm th}$ percentile values derived from bootstrap resampling of our data.

particular colour–stellar mass range (see the bottom panels of Figure 4). Figure 5 shows the percentage of PSGs per $10^{0.5}$ $M_\odot$ bins. The average percentage of PSGs in the log $M_\star$ bins between 9.5 and 10.5 $M_\odot$ is $\sim$ 8 times greater than that between the log $M_\star$ bins between 10.5 and 11.5 $M_\odot$ (with a 3σ significance). The uncertainties in the stellar masses are dominated by the uncertainties in the stellar population models and can be up to $10^{0.3}$ $M_\odot$ in stellar masses (e.g. Conroy et al. 2009).

One possible reason for the lack of high mass PSGs is likely to be because our sample is restricted to a very local volume. As such, the probability of finding massive galaxies in such a local volume is much less than at higher redshifts. Galaxies with log stellar masses greater than 11.5 account for only 3.8% of the entire galaxy sample. In addition, high-redshift surveys of E+A galaxies are not as sensitive to smaller (and fainter) galaxies. As such, the E+A galaxies found at $z \sim 0.1$ are most likely the biggest and brightest types of post-starburst galaxies. For example, the PSG sample at $z = 0.8$ in Yan et al. (2009) have stellar masses greater than $10^{10.6}$ $M_\odot$. In addition, low redshift PSGs are also more closely associated to less massive blue galaxies than high redshift PSGs which are more similar to massive red galaxies (e.g. Yan et al. 2009). Therefore, it is not surprising that our local sample of PSGs is dominated by low mass objects.

In addition to the apparent stellar mass limit of our PSG population, the bottom panels of Figure 4 also show that a significant fraction (61%) of our PSG sample reside within the "green valley", while 31% and 8% reside in the "blue cloud" ($u-r < 1.8$) and the "red sequence", respectively. Similarly, we find that the percentage of PSGs within the "green valley" (0.6%) is 17 times and 6 times greater than the fraction of PSGs within the "red sequence" and the "blue cloud", respectively. Hence, we propose that local PSGs occupy a well-defined position in the low-mass end of the "green valley". Consistent with the idea of galaxy formation downsizing, we postulate that local PSGs will transform into passively-evolving "red" galaxies and contribute towards the build-up of the low-mass end of the "red sequence" if star formation has indeed ceased.

3.3 Environment

Using the adaptive Gaussian environment parameter, $\rho_{\rm g}$ (which provides a measure of the number and proximity of galaxies around a point in space, see Schawinski et al. 2007), we study the environment properties of our PSG sample. Low, medium and high density environments are described by $\rho_{\rm g} < 0.21$, $0.21 < \rho_{\rm g} < 0.58$ and $\rho_{\rm g} > 0.58$ respectively (Schawinski et al. 2007). The low density class of environment can be likened to the galaxy field environment.

Table 3. Fractions of galaxies in three different environment classes for different types of galaxies.

Galaxy type	$\rho_{\rm g} < 0.21$	$0.21 < \rho_{\rm g} < 0.58$	$\rho_{\rm g} > 0.58$
Early-type	45% (4034)	29% (2561)	26% (2333)
Intermediate	53% (11866)	27% (6022)	20% (4592)
Late-type	56% (9124)	28% (4555)	16% (2566)
PSG	50% (40)	26% (21)	24% (19)

Similarly, the medium and high density classes can be compared to the group (or cluster outskirts) and cluster environments, respectively.

We find that 50% of our sample reside in the low density environment, while 26% and 24% reside in the medium and high density environments, respectively. In high density environments, the fraction of PSGs is similar to that of early-types, while in low density environments, the fraction of PSGs is in between that of intermediate- and early-type galaxies. As can be seen from Table 3, the number fractions of early- and late-type galaxies in the low and high density environments differ by $\sim$10% whereby a greater fraction of early-types are found in high density environments and a greater fraction of late-types are found in low density environments. This greater fraction of early-type galaxies at higher densities recapitulates the well-known morphology–density relation found by Dressler (1980) and more recent studies such as Bamford et al. (2009). Similar to the PSG sample, the intermediate-type galaxies appear to have fractions which are in between those found for early- and late-types. In addition, the fractions of galaxies residing in medium density environments are roughly the same regardless of galaxy types.It should be noted that KS tests comparing the $\rho_{\rm g}$ distributions of different galaxy types confirm these results. Hence, we find that the PSG distributions across all three environment classes are similar to those of the early- and intermediate-type galaxies. This is consistent with the fact that $\sim$ 90% of the PSG sample consists of galaxies classified as early- or intermediate-type galaxies. Our results are also consistent with those of Blake et al. (2004) who found that the local environments of E+A galaxies follow that of the general galaxy population.

4 DISCUSSION

Our results show that local post-starburst galaxies represent one population of galaxies which currently occupies a well-defined position in the low-stellar-mass end of the "green valley" and is rapidly transitioning onto the low-mass end of the "red sequence" unless star formation resumes within the transitioning period of $\sim$ 1 Gyr. The duration within which the individual PSG spends in the "green valley" is probably only on the order of $\sim$ 1 Gyr (the timescale for the fading of the Lyman continuum from the current generation of young stars) because structurally, the stellar concentration of the PSGs within the "green valley" already closely resemble those of low-mass early-type galaxies even though star formation has only been truncated recently. Our transition timescale concurs with recent findings of transition times on the order of $\sim$ 1 Gyr between the "blue cloud" and the "red sequence" (e.g. Kaviraj et al. 2011, 2007; Schawinski et al. 2007). These results are consistent with the idea of downsizing in the sense that larger objects have mostly been formed at earlier epochs, while smaller objects are still being formed at later epochs. Our results are therefore comparable to those of Wild et al. (2009) who found the mass density of PSGs to be 230 times lower at $z \sim 0.07$ than at $z \sim 0.7$.

Current galaxy evolution models often suggest that feedback from an active galactic nuclei (AGN) could provide the means to quench and truncate the star formation history of a massive galaxy (e.g. Silk & Rees 1998; Kaviraj et al. 2005; Croton et al. 2006). Incidentally, our observation of a stellar mass limit in our PSG sample coincides with the findings of Schawinski et al. (2010) who found that the AGN duty cycle peaks at the low mass-end of the "green valley" and that the low-mass early-type AGN hosts appear to have post-starburst properties. However, apart from two PSGs which exhibit spectral properties of LINERs, we do not observe any spectral signatures of AGN within our PSG sample.

The connection between AGN and merger/interactions have been discussed in the context of mergers inducing in-flows of gas that fuel star formation and the black hole (in the central regions; e.g. Canalizo et al. 2006), while feedback from the AGN is predicted to quench star formation by re-heating the cold gas and expelling much of it in AGN-driven winds (e.g. Di Matteo et al. 2005; Thacker et al. 2006). Tremonti et al. (2007) found evidence for these winds in 10 out of 14 PSGs at $z = 0.6$. They hypothesised that the observed gas outflows in these galaxies suggest that AGN feedback may play a role in quenching star formation in PSGs. Compared to the PSG sample of Tremonti et al. (2007), our local PSGs are redder and not as massive. Therefore, following the results of Yan et al. (2009) and Wild et al. (2009), we hypothesise that the evolution of our local PSG sample is likely to be different to that of PSGs at higher redshifts. Consistent with the results of Kaviraj et al. (2007), it is unlikely that AGN feedback will be a dominant quenching process for star formation in local PSGs.

5 SUMMARY

In this paper, we have presented a study of local post-starburst galaxies (PSGs) using the photometric and spectroscopic observations from SDSS in conjunction with the results from the Galaxy Zoo 1 project. We find that:

- The local population of PSGs occupy a well-defined space on the colour–stellar mass diagram, most notably in the low-mass end of the green valley below the transition mass (log $M_\star < 10.5$ M$_\odot$; Kauffmann et al. 2003) thought to be the mass division between low-mass star-forming galaxies and high-mass passively-evolving bulge-dominated galaxies. Consistent with the idea of galaxy formation downsizing where smaller galaxies form at later epochs, we think that the local PSGs will contribute to the build-up of the low-mass end of the red sequence if star formation has indeed ceased in these galaxies.
- Consistent with previous studies (e.g. Blake et al. 2004), we find that local environment of local PSGs follow that of the general galaxy population within the same volume.
- Using the morphological classifications from Galaxy Zoo, we are able to study the distributions of morphologies in our PSG sample in comparison to those of 47,573 galaxies in our full galaxy sample within the same local volume. Although a majority of our local PSG sample appears to have intermediate-type morphologies which are neither early- nor late-type morphologies, we find that the stellar structural morphology (as described by `fracDev`) of the local "green valley" PSGs to be very similar to that of low-mass early-type galaxies in the "red sequence" even though star formation has only recently ceased. Therefore, unless star formation resumes, we hypothesize that the local PSGs will evolve out

of the "green valley" in ~ 1 Gyr onto the "red sequence" as soon as the young stellar population from the most recent episode of star formation fades.

Acknowledgments. Galaxy Zoo acknowledges support from The Leverhulme Trust. OIW is the recipient of a Super Science Fellowship from the Australian Research Council. Support for the work of KS was provided by NASA through Einstein Postdoctoral Fellowship grant number PF9-00069 issued by the Chandra X-ray Observatory Center, which is operated by the Smithsonian Astrophysical Observatory for and on behalf of NASA under contract NAS8-03060. KLM acknowledges funding from the Peter and Patricia Gruber Foundation as the 2008 Peter and Patricia Gruber Foundation International Astronomical Union Fellow, from a 2010 Leverhulme Trust Early Career Fellowship and from the University of Portsmouth and SEPnet (www.sepnet.ac.uk). The authors also thank the anonymous referee for the constructive comments which has improved this paper.

REFERENCES

Abazajian K. N., Adelman-McCarthy J. K., Agüeros M. A., Allam S. S., Allende Prieto C., An D., Anderson K. S. J., Anderson S. F., et al. 2009, ApJS, 182, 543
Abraham R. G., Smecker-Hane T. A., Hutchings J. B., Carlberg R. G., Yee H. K. C., Ellingson E., Morris S., Oke J. B., et al. 1996, ApJ, 471, 694
Baldry I. K., Balogh M. L., Bower R. G., Glazebrook K., Nichol R. C., Bamford S. P., Budavari T., 2006, MNRAS, 373, 469
Baldry I. K., Glazebrook K., Brinkmann J., Ivezić Ž., Lupton R. H., Nichol R. C., Szalay A. S., 2004, ApJ, 600, 681
Balogh M. L., Morris S. L., Yee H. K. C., Carlberg R. G., Ellingson E., 1999, ApJ, 527, 54
Bamford S. P., Nichol R. C., Baldry I. K., Land K., Lintott C. J., Schawinski K., Slosar A., Szalay A. S., et al. 2009, MNRAS, 393, 1324
Bekki K., Shioya Y., Couch W. J., 2001, ApJ, 547, L17
Blake C., Pracy M. B., Couch W. J., Bekki K., Lewis I., Glazebrook K., Baldry I. K., Baugh C. M., et al. 2004, MNRAS, 355, 713
Caldwell N., Rose J. A., 1997, AJ, 113, 492
Calzetti D., Armus L., Bohlin R. C., Kinney A. L., Koornneef J., Storchi-Bergmann T., 2000, ApJ, 533, 682
Canalizo G., Stockton A., Brotherton M. S., Lacy M., 2006, "New Astronomy Reviews", 50, 650
Conroy C., Gunn J. E., White M., 2009, ApJ, 699, 486
Couch W. J., Ellis R. S., Sharples R. M., Smail I., 1994, ApJ, 430, 121
Couch W. J., Sharples R. M., 1987, MNRAS, 229, 423
Croton D. J., Springel V., White S. D. M., De Lucia G., Frenk C. S., Gao L., Jenkins A., Kauffmann G., Navarro J. F., Yoshida N., 2006, MNRAS, 365, 11
Darg D. W., Kaviraj S., Lintott C. J., Schawinski K., Sarzi M., Bamford S., Silk J., Proctor R., et al. 2010, MNRAS, 401, 1043
Di Matteo T., Springel V., Hernquist L., 2005, Nat, 433, 604
Dressler A., 1980, ApJ, 236, 351
Dressler A., Gunn J. E., 1983, ApJ, 270, 7
Dressler A., Gunn J. E., 1992, ApJS, 78, 1
Dressler A., Oemler Jr. A., Butcher H. R., Gunn J. E., 1994, ApJ, 430, 107
Dressler A., Oemler Jr. A., Poggianti B. M., Smail I., Trager S., Shectman S. A., Couch W. J., Ellis R. S., 2004, ApJ, 617, 867
Dressler A., Smail I., Poggianti B. M., Butcher H., Couch W. J., Ellis R. S., Oemler Jr. A., 1999, ApJS, 122, 51
Driver S. P., Allen P. D., Graham A. W., Cameron E., Liske J., Ellis S. C., Cross N. J. G., De Propris R., et al. 2006, MNRAS, 368, 414
Drory N., Bundy K., Leauthaud A., Scoville N., Capak P., Ilbert O., Kartaltepe J. S., Kneib J. P., et al. 2009, ApJ, 707, 1595
Fabricant D. G., McClintock J. E., Bautz M. W., 1991, ApJ, 381, 33
Goto T., 2004, A&A, 427, 125
Goto T., 2005, MNRAS, 357, 937
Goto T., 2007, MNRAS, 381, 187
Goto T., Okamura S., Sekiguchi M., Bernardi M., Brinkmann J., Gómez P. L., Harvanek M., Kleinman S. J., et al. 2003, PASJ, 55, 757
Hunter D. A., 1994, AJ, 107, 565
Hunter D. A., Gallagher III J. S., 1990, ApJ, 362, 480
Kannappan S. J., Guie J. M., Baker A. J., 2009, AJ, 138, 579
Kauffmann G., Heckman T. M., White S. D. M., Charlot S., Tremonti C., Peng E. W., Seibert M., Brinkmann J., et al. 2003, MNRAS, 341, 54
Kauffmann G., White S. D. M., Heckman T. M., Ménard B., Brinchmann J., Charlot S., Tremonti C., Brinkmann J., 2004, MNRAS, 353, 713
Kaviraj S., Devriendt J. E. G., Ferreras I., Yi S. K., 2005, MNRAS, 360, 60
Kaviraj S., Kirkby L. A., Silk J., Sarzi M., 2007, MNRAS, 382, 960
Kaviraj S., Schawinski K., Silk J., Shabala S. S., 2011, MNRAS, pp 936–+
Kennicutt Jr. R. C., 1992, ApJ, 388, 310
Kennicutt Jr. R. C., 1998, ARA&A, 36, 189
Land K., Slosar A., Lintott C., Andreescu D., Bamford S., Murray P., Nichol R., Raddick M. J., et al. 2008, MNRAS, 388, 1686
Lintott C., Schawinski K., Bamford S., Slosar A., Land K., Thomas D., Edmondson E., Masters K., Nichol R., Raddick J., Szalay A., Andreescu D., Murray P., Vandenberg J., 2010, ArXiv e-prints
Lintott C. J., Schawinski K., Slosar A., Land K., Bamford S., Thomas D., Raddick M. J., Nichol R. C., et al. 2008, MNRAS, 389, 1179
MacLaren I., Ellis R. S., Couch W. J., 1988, MNRAS, 230, 249
Maraston C., 1998, MNRAS, 300, 872
Maraston C., 2005, MNRAS, 362, 799
Martin C. L., 1998, ApJ, 506, 222
Martin D. C., Small T., Schiminovich D., Wyder T. K., Pérez-González P. G., Johnson B., Wolf C., Barlow T. A., et al. 2007, ApJS, 173, 415
Masters K. L., Nichol R., Bamford S., Mosleh M., Lintott C. J., Andreescu D., Edmondson E. M., Keel W. C., et al. 2010, MNRAS, 404, 792
Newberry M. V., Boroson T. A., Kirshner R. P., 1990, ApJ, 350, 585
Poggianti B. M., Smail I., Dressler A., Couch W. J., Barger A. J., Butcher H., Ellis R. S., Oemler Jr. A., 1999, ApJ, 518, 576
Sarzi M., Falcón-Barroso J., Davies R. L., Bacon R., Bureau M., Cappellari M., de Zeeuw P. T., Emsellem E., et al. 2006, MNRAS, 366, 1151

Schawinski K., Kaviraj S., Khochfar S., Yoon S., Yi S. K., Deharveng J., Boselli A., Barlow T., et al. 2007, ApJS, 173, 512
Schawinski K., Thomas D., Sarzi M., Maraston C., Kaviraj S., Joo S., Yi S. K., Silk J., 2007, MNRAS, 382, 1415
Schawinski K., Urry C. M., Virani S., Coppi P., Bamford S. P., Treister E., Lintott C. J., Sarzi M., et al. 2010, ApJ, 711, 284
Silk J., Rees M. J., 1998, A&A, 331, L1
Strateva I., Ivezić Ž., Knapp G. R., Narayanan V. K., Strauss M. A., Gunn J. E., Lupton R. H., Schlegel D., et al. 2001, AJ, 122, 1861
Strauss M. A., Weinberg D. H., Lupton R. H., Narayanan V. K., Annis J., Bernardi M., Blanton M., Burles S., et al. 2002, AJ, 124, 1810
Thacker R. J., Scannapieco E., Couchman H. M. P., 2006, ApJ, 653, 86
Tran K., Franx M., Illingworth G. D., van Dokkum P., Kelson D. D., Magee D., 2004, ApJ, 609, 683
Tremonti C. A., Moustakas J., Diamond-Stanic A. M., 2007, ApJ, 663, L77
Wei L. H., Kannappan S. J., Vogel S. N., Baker A. J., 2010, ApJ, 708, 841
Wild V., Walcher C. J., Johansson P. H., Tresse L., Charlot S., Pollo A., Le Fèvre O., de Ravel L., 2009, MNRAS, 395, 144
Yamauchi C., Yagi M., Goto T., 2008, MNRAS, 390, 383
Yan R., Newman J. A., Faber S. M., Coil A. L., Cooper M. C., Davis M., Weiner B. J., Gerke B. F., et al. 2009, MNRAS, 398, 735
Yang Y., Zabludoff A. I., Zaritsky D., Mihos J. C., 2008, ApJ, 688, 945
York D. G., Adelman J., Anderson Jr. J. E., Anderson S. F., Annis J., Bahcall N. A., Bakken J. A., Barkhouser R., et al. 2000, AJ, 120, 1579